HHS Public Access

Author manuscript

J Control Release. Author manuscript; available in PMC 2016 June 28.

Published in final edited form as:

J Control Release. 2015 June 28; 208: 59–66. doi:10.1016/j.jconrel.2015.02.001.

Polypeptide-based nanogels co-encapsulating a synergistic combination of Doxorubicin with 17-AAG show potent anti-tumor activity in ErbB2-driven breast cancer models

Swapnil S. Desale[1,#], **Srikumar M. Raja**[2,*,#], **Jong Oh Kim**[1,5], **Bhopal Mohapatra**[2], **Kruti S. Soni**[1], **Haitao Luan**[2], **Stetson H. Williams**[2], **Tim A Bielecki**[2], **Dan Feng**[2], **Matthew Storck**[2], **Vimla Band**[3], **Samuel M. Cohen**[4], **Hamid Band**[2,*], and **Tatiana K. Bronich**[1,*]

[1]Department of Pharmaceutical Sciences and Center for Drug Delivery and Nanomedicine, University of Nebraska Medical Center (UNMC), Omaha, NE 68198

[2]Eppley Institute for Research in Cancer and Allied Diseases, UNMC

[3]Department of Genetics, Cell Biology and Anatomy, UNMC

[4]Department of Pathology and Microbiology, UNMC

[5]College of Pharmacy, Yeungnam University, Gyeongsan, 712-749, South Korea

1. Introduction

The receptor tyrosine kinase ErbB2 (also known as Her2/Neu) is overexpressed in 20–25 % of breast cancer patients [1–5]. Oncogenic ErbB2 signaling results in hyperproliferation of the cells, increases cell survival and promotes invasion and metastasis [6, 7]. The anti-ErbB2 monoclonal antibody, Trastuzumab (Herceptin™)[8], in combination with chemotherapy is currently used for treatment of ErbB2-overexpressing breast cancers, following surgical removal of the primary tumor [5, 8, 9]. However, many patients either do not respond to Trastuzumab-based therapies or relapse during the course of the treatment, necessitating the development of newer therapeutics [8]. ErbB2 depends on heat shock protein 90 (HSP90) association for stability and, among client proteins of the chaperone, ErbB2 is perhaps the most sensitive to HSP90 inhibition [10]. HSP90 inhibitors (such as the ansamycin antibiotic, Geldanamycin and related molecules like 17-AAG) have shown significant promise in pre-clinical models of ErbB2-driven breast cancer as well as initial phase I/II clinical trials [11–13]. The mechanism involves attenuation of oncogenic signaling via degradation of ErbB2 as well as other critical downstream signaling mediators in the pathway, which include phospho-Akt and c-Raf. In a cancer cell, these signaling molecules are strongly dependent on HSP90 to maintain their stability [14–16]. Since numerous oncoproteins have been

*Correspondence to: SMR (srikumar.raja@northwestern.edu; Ph: 630-674-0103); HB (hband@unmc.edu; Ph: 402-559-8572); TKB (tbronich@unmc.edu; Ph: 402-559-9351).

#These authors contributed equally to this work.

identified as HSP90 clients, inhibition of Hsp90 functions affects multiple oncogenic substrates simultaneously and represents an appealing molecular target for combination drug therapy [17]. In a recently completed phase II study of 17-AAG and trastuzumab, an overall clinical benefit (including stable disease) was seen in 57% of the patients with ErbB2-positive metastatic breast cancer progressing on trastuzumab [13]. It has also been reported that inhibition of Hsp90 with 17-AAG sensitizes different cancer cell lines to DNA damage response mediated cellular senescence [18]. It was shown that the 17AAG pre-treatment followed by doxorubicin (Dox) treatment exhibited senescence-like characteristics such as increased nucleus to cytoplasm ratio and cell cycle arrest in the pre-clinical evaluation [18–20]. These data suggest that combination chemotherapy using co-administration of 17-AAG with a Dox-based regimen can be a potential therapy for cancer especially ErbB2-positive breast cancer [18].

Combining drugs in one delivery carrier is a well-suited strategy for controlling the pharmacokinetics and co-delivery of the desired drug ratio in vivo [21, 22]. The drug loading and structure of such carriers can be tuned to control the drug release rates, maximize the therapeutic potency and minimize drug-associated toxicities. However, co-incorporation of drug molecules with different physicochemical properties, such as hydrophilic Dox and hydrophobic 17-AAG, has been challenging. We have recently described biodegradable polymeric nanogels (NGs) based on poly(ethylene glycol)-*b*-poly(L-glutamic acid) (PEG-*b*-PGA) with pendant phenylalnine functionalities [23]. Such NGs have multiple hydrophobic domains formed by phenylalanine moieties within the cross-linked PGA polyion cores surrounded by a hydrophilic PEG shell. Herein, we explored these novel NGs for co-encapsulation of 17-AAG and Dox. The potency of this co-delivery system was evaluated in a panel of human breast cancer lines and in an ErbB2-driven orthotopic xenograft model. We demonstrate that NGs-based co-delivery of synergistic combination of 17-AAG and Dox exhibited superior antitumor efficacy compared to a combination of free drugs. The implications of our results may support a new platform for delivery of combinations of HSP90 inhibitors with cytotoxic agents for treatment of various types of cancers.

2. Materials and Methods

Materials

Poly(ethylene glycol)-*b*-poly(L-glutamic acid) (PEG-*b*-PGA) diblock copolymer (M_w/M_n = 1.38, MW 27,500) was purchased from Alamanda Polymers, Inc (Madison, AL, USA). The block lengths were 114 and 150 repeating units for PEG and PGA, respectively. L-phenylalanine methyl ester (PME), calcium chloride, cystamine, 1-(3-dimethylaminopropyl)-3-ethylcarbodiimide hydrochloride (EDC) and ethylenediaminetetraacetic acid (EDTA) were obtained from Sigma-Aldrich (St Louis, MO). Doxorubicin hydrochloride was kindly provided by Dong-A Pharmaceutical Company, South Korea. Fetal bovine serum (FBS) (both dialyzed and heat inactivated), DMEM and RPMI 1640 media and Lysotracker™ (green) were purchased from Invitrogen Inc (Carlsbad, CA). Bovine serum albumin (BSA) and NUNC™ chambered glass coverslips for live cell imaging were purchased from Fisher Scientific (Waltham, MA). MTT reagent (3-

(4,5-Dimethylthiazol-2-yl)-2,5-diphenyltetrazolium bromide) was purchased from Research Products International (Prospect, IL). All other chemicals were of reagent grade and used without further purification. The following primary antibodies were used in this study: anti-human-ErbB2 mouse monoclonal (ErbB2) raised against the C-terminal amino acid residues (1242–1255), used for Western blotting studies, were purchased from BD Pharmingen™ (San Diego, CA); for flow cytometry and immunofluorescence studies, the goat anti-human-ErbB2 polyclonal antibody (AF1129) was from R&D Systems (Minneapolis, MN); the mouse monoclonal anti-phosphotyrosine (anti-pY; 4G10) was kindly provided by Dr. Brian Druker (Oregon Health & Science University, Portland, OR); the mouse monoclonal anti-Hsc70 antibody was from Santa Cruz Biotechnology Inc. (Santa Cruz, CA).

Synthesis of nanogels

The hydrophobic phenylalanine functionalities were introduced in PEG-*b*-PGA copolymer by polymer-analogous modification of the PGA segment with PME using carbodiimide chemistry as we previously described [23]. The degree of PME grafting in resulting PEG-*b*-PPGA copolymer was 30% as determined by 1H-NMR analysis. Nanogels were prepared as described earlier [23] by using block ionomer complex PEG-*b*-PPGA/Ca^{2+} at a molar ratio of $[Ca^{2+}]/[COO^{-}] = 1.5$ with further cross-linking by cystamine and EDC ([EDC]/[cystamine] = 2; [COOH]/[EDC] = 5) at r.t., overnight. Byproducts of the cross-linking reaction and metal ions were removed by exhaustive dialysis of the reaction mixtures, first against 0.5% aqueous ammonia with EDTA and then against distilled water.

Drug loading

Dox-encapsulated nanogels (Dox/NG) were prepared by adding Dox to an aqueous dispersion of NGs at the feeding ratio of $R = [Dox]/[COO^{-}] = 0.25$, for 24h at pH 7.0. Unbound Dox was separated by centrifugal filtration on drug-pretreated Amicon YM-30 filters. 17-AAG was solubilized into the hydrophobic domains of NGs using an extraction method [24]. According to this method, a thin film of 17-AAG (prepared by evaporation of a methanol solution of 17-AAG) was incubated with aqueous dispersion of NGs or Dox/NG (24 h, r.t.). Unincorporated 17-AAG was removed by filtration. Dox was assayed by UV spectrophotometry (ε_{488} = 11,500 M^{-1} cm^{-1} in water) [25]. The amount of 17-AAG incorporated into NGs was quantified via reverse-phase HPLC using an Agilent Eclipse XDB C18 5 μm column (250 mm × 4.6mm) and Agilent 1200 HPLC system. Mobile phase was composed of 10 mM ammonium acetate containing 0.1% (v/v) acetic acid (pH 4.8) and 50% acetonitrile and was applied at a flow rate of 1 mL/min. Detection wavelength was 334 nm. Drug loading capacity was calculated as percent ratio of mass of incorporated drug to total mass of drug-loaded NGs without water.

Physicochemical characterization of the nanogels

The effective hydrodynamic diameter (D_{eff}) and ζ-potential of NGs were determined using a Malvern Zetasizer (Malvern Instruments Ltd., Malvern, UK). All measurements were performed in automatic mode at 25°C. Software provided by the manufacturer was used to calculate size, polydispersity indices and ζ-potential of NGs. All measurements were performed at least in triplicate to calculate the mean values ± SD.

Drug release studies

Drug release from NGs was examined in PBS (pH 7.4, 0.14M NaCl) by dialysis method using a membrane with 3500 Da cutoff. The concentrations of 17-AAG and Dox released were determined by HPLC and UV spectrophotometry, respectively, and expressed as a percentage of the total 17-AAG or Dox available vs. time.

Cell culture

The ErbB2-overexpressing cell lines used in this study were 21MT-1 and BT-474. MCF-7 cells were used as a representative ErbB2-low cell line for comparison. The ErbB2-overexpressing breast cancer cell line 21MT-1 was established by Band et al [26] and has been previously described. BT-474 and MCF-7 cell lines were obtained from the American Type Culture Collection (ATCC). All cell lines were maintained as previously described [27, 28].

Confocal microscopy on live cells

Cellular uptake and localization studies of (Dox+17-AAG)/NG were conducted using live cell confocal microscope (Carl Zeiss LSM 510 Meta, Peabody, MA). 21MT-1 human breast cancer cells (1×10^6/chamber) were grown in live cell chambers (Fischer Scientific, Waltham, MA) for two days (37°C, 5% CO_2) and exposed to (Dox+17-AAG)/NG for 30 min followed by incubation with Lysotracker Green for 5 min. After exposure cells were washed with PBS and kept in complete media prior to visualization by live cell confocal imaging (Carl Zeiss LSM 510 Meta, Peabody, MA).

ErbB2 degradation

ErbB2-overexpressing cells plated in 6-well plates were treated with free 17-AAG or the drug-loaded NG formulations, following which the samples were lysed using RIPA lysis buffer, supplemented with protease and phosphatase inhibitors. Analysis of the kinetics and dose-response of ErbB2 degradation induced by free 17-AAG or 17-AAG/NG formulations were done using SDS-PAGE/WB [27, 28].

In vitro cytotoxicity studies

Cytotoxicity of drug-loaded NGs was assessed in 21MT-1, BT-474, and MCF-7 cells by a standard MTT assay [29]. Briefly, cells were seeded in 96-well plates (5,000 cells/well) and allowed to adhere for 24 h prior to the assay. Cells were exposed to various concentrations of free drugs (0 – 10 μg/mL Dox or 0 – 17.2 μM 17-AAG), drug-loaded NGs for 48 h at 37 °C. Cells were then washed with PBS and MTT indicator dye (25 μL, 5 mg/mL) was added to each well and the cells were incubated for 2 h at 37°C in the dark. A solution of 50% DMF-20% SDS (100 μL) was added to each well and kept overnight at 37 °C. Absorbance was read at 570 nm using a plate reader (SpectraMax M5, Molecular Devices Co., USA). Cell survival rates were calculated as normalized to control untreated wells. All measurements were taken eight times. Based on the results of the test, the IC_{50} values and synergic effects of Dox and 17-AAG in these cells were calculated by using CampuSyn Software (Combosyn, USA). Combination index (CI) values less than 1 indicate synergism

while CI values equal or more than 1 represent additive and antagonistic effects of drug combination, respectively.

Animal Studies

All animal studies were conducted in accordance with an approved protocol by the University of Nebraska Medical Center Institutional Animal Care and Use Committee (IACUC). 10^7 BT-474 cells (an ErbB2 overexpressing human breast cancer cell line) reconstituted in 50% Matrigel (BD Biosciences, California) in media were injected directly into the mammary fat pad of 4–6 week old female Athymic NCr-nu/nu mice (NCI, Fredrick National Lab, Fredrick, MD). 17-β-Estradiol pellets (0.72mg/pellet; 60 day release; Innovative Research of America, Sarasota, Fl) were implanted subcutaneously on the lateral side of the neck of the mice three days prior to the injection of the tumor cells. The mice were randomized when the average tumor size reached 100–200 mm^3 (14 days after tumor inoculation) into treatment groups (n = 10), and treated with Dox/NG or 17-AAG/NG or (Dox + 17-AAG)/NG or combination of free Dox and 17-AAG in the same ratio as in (Dox + 17-AAG)/NG at an equivalent dose of 6 mg/kg Dox, or 1 mg/kg 17-AAG or (6 mg/kg Dox + 1 mg/kg 17-AAG) or 5% dextrose solution. 17-AAG was formulated in Chemophor-EL : propylene glycol : ethanol (2:3:5 by volume) mixture for injections as a component of the free drug combination. Treatments were administered via tail vein injections at 4-day intervals. Animal body weight and tumor volume were monitored every second day. Tumor volume ($V = 0.5 \times L \times W^2$) was estimated by measuring two orthogonal diameters (longer dimension: L, and smaller dimension: W) of the tumor using electronic calipers. The T/C values were determined from changes in average tumor volumes of drug-treated groups relative to control group. Animals were sacrificed when tumor volume exceeded 3000 mm^3, greatest tumor dimension exceeded 20 mm, tumor became necrotic, or animal exhibited a body weight loss of more than 20%. All other animals were sacrificed by day 23.

Cell proliferation assay

Tumors from mice that received different treatments were excised at day 14 (3 mice per group). The tumors were dissected and fixed in 10% neutral buffered formalin. Then, the tissues were processed routinely into paraffin, sectioned at a thickness of 4 μm. Proliferation was detected using an antibody against Ki-67 (Biocare medical, CA) followed by visualization by incubation with DAB+ (brown, for Ki-67) for 2 min. After rinsing with distilled water, the sections were counterstained with hematoxylin. For quantification of Ki-67 expression, the number of Ki-67 positive cells was determined (Image J) in 5 random high power fields (20× magnification) and divided by the total number of cells for each field of slice.

Histopathology analysis

Specific tissues (liver, spleen, heart kidney and lung) were fixed in buffered formalin and were sectioned, inserted into tissue cassettes, dehydrated in 70% ethanol overnight, and paraffin embedded (UNMC Tissue Sciences Facility, Omaha, NE). Serial 5 μm sections were stained with hematoxylin and eosin (H&E). For histopathological diagnosis, H&E-stained slides were examined by light microscopy.

Statistical analysis

Statistical comparisons for in vitro studies were carried out using Student t-test. For the antitumor study and toxicity studies, group means for tumor volume and body weights were evaluated using repeated measures analysis of variance. Survival was estimated using Kaplan–Meier analysis and compared using log-rank test. *P* values less than 0.05 were considered significant. Analysis of variance and Kaplan–Meier analysis with log-rank test were performed using GraphPad Prism 5 (GraphPad Software, Inc.).

3. Results and Discussion

Preparation and characterization of nanogels co-encapsulating 17-AAG and Dox

PEG-b-PGA diblock copolymer, in which about 30% of GA units were modified with hydrophobic phenylalanine moieties, were utilized for the synthesis of biodegradable NGs. NGs were prepared as previously described by template-assisted method involving condensation of these hydrophobically modified block copolymers by Ca^{2+} ions into polyion complex micelles, followed by chemical cross-linking of the polyion chains in their cores [23]. A cleavable diamine crosslinker, cystamine, was used for synthesis of the NGs with targeted density of cross-links of 20% (based on the molar ratio of cross-linker to carboxylic acid groups of the GA residues). The resulting core-shell NGs displayed an effective diameter of about 80 nm (ζ-potential = −45 mV) and were uniform (monomodal, narrow size distribution) as determined by dynamic light scattering (DLS). We have previously shown that water-soluble anticancer drugs such as Dox or cisplatin can be encapsulated with high loading efficiency into NGs ionic cores through electrostatic or coordination interactions [23, 30]. In addition, it was demonstrated that hydrophobic domains formed by phenylalanine moieties within the ionic cores of NGs could solubilize hydrophobic molecules and, therefore, such hybrid NGs provide unique opportunities for combinational drug delivery especially for the drugs that possess different solubility.

It has been reported that HSP90 inhibitors including 17-AAG show additive or synergistic activities with agents commonly used to treat advanced malignancies [31–35]. Particularly, it was demonstrated that 17-AAG synergistically enhances the antiproliferative effect of Dox chemotherapy. The mechanism of synergy is thought to involve 17-AAG-mediated degradation of many of the proteins required for DNAdamage response (such as ATM/ATR or Chk1 kinase), the activities of which are dependent on HSP90 chaperoning function [36]. Additionally, in the case of ErbB2-driven cancers, given the ability of 17-AAG to attenuate hyperactive ErbB2 signaling (which is known to be involved in transcriptional upregulation of genes encoding DNA-damage repair enzymes) [37], it can potentially enhance the cytotoxic effect of Dox-induced DNA damage. Based on these considerations, we attempted to encapsulate both hydrophilic Dox and hydrophobic 17-AAG into NGs with hydrophobically modified ionic cores. At first, Dox was incubated with aqueous dispersion of NGs for 24 h at pH 7.0. As expected, the net negative charge and particle size of Dox-loaded NGs (Dox/NG) decreased upon Dox loading due to progressive neutralization and condensation of the PGA segments upon Dox binding to carboxylate groups (Table 1).

Under these conditions Dox loading capacity of NGs was about 18% w/w as measured by UV-Vis spectroscopy. Binary drug formulation, (Dox+17-AAG)/NG, was prepared by solubilization of 17-AAG into Dox/NG using an extraction method. A similar procedure was used to prepare single 17-AAG/NG formulations. 17-AAG content was determined by HPLC. Comparable loading capacity values for 17-AAG were achieved for NGs with binary drug combination (3.1%) and for single 17-AAG/NG (2.7%). A total loading capacity of NGs for the binary drug combination was about 21% w/w and corresponds to 6:1 Dox/17-AAG molar ratio. The physicochemical characteristics of drug-loaded NGs are presented in Table 1. The size and ζ-potential of the (Dox+17-AAG)/NG were comparable to those of Dox/NG indicating that an inclusion of 17-AAG into the NG cores did not affect the macroscopic characteristics of Dox-loaded NGs. Importantly, single and binary drug formulations exhibited excellent stability in aqueous dispersions: no changes in sizes and loading capacities were observed for at least two months.

The release profile of the encapsulated drug from the nanocarrier is crucial for the synergy of the drugs [20]. Profound synergistic effects were observed when 17-AAG was administered prior to Dox while the sequence of Dox before 17-AAG had less cytotoxic activity in vitro [20, 34]. Figure 1 shows the cumulative release profiles of Dox and 17-AAG from the NGs at physiological pH and temperature.

As seen from these data, sustained but temporally distinct release of Dox and 17-AAG was observed. For example, during 12 hrs (Dox+17-AAG)/NG released ~ 90% of loaded 17-AAG and only ~ 17% of loaded Dox. Notably, 17-AAG release was much faster than that of Dox, which is expected since 17-AAG is physically entrapped into the hydrophobic domains in the cores of NGs. In contrast, Dox binds with PGA chains through electrostatic and van der Waals interactions and its release usually proceeds via ion exchange reactions, thus delaying its liberation from the NGs. Furthermore, intermolecular interactions between the anthraquinone moiety of Dox and phenylalanine hydrophobic domains of NGs in combination with more compact cross-linked core [23] could account for the delayed and controlled release of Dox from the NGs. It is also interesting that the individual drug release rates practically did not change for binary drug formulations compared to the single drug-loaded NGs (Fig. 1).

Intracellular uptake of drug-loaded NGs

NG-based drug-carriers (made of biodegradable materials) are designed to be internalized by cancer cells via the endocytic pathway and disintegrate under lysosomal pH and reducing environment, to release the anticancer drugs into the cytosol. It was important to confirm that the (Dox+17-AAG)/NG uptake into the cells was indeed a result of internalization of intact drug-loaded NGs and subsequent drug release. We therefore compared the kinetics of uptake of free Dox or Dox/NG into 21MT-1 cells, monitoring the intrinsic fluorescence of Dox, using a fluorescence microscope. Images were taken using a 10× and a 20× microscope lens.

As shown in Fig. 2, the free Dox, which rapidly partitions across the plasma membrane, was found within the nuclei of cells as early as 15 min. On the other hand, the fluorescence of Dox followed by treatments with Dox/NG (at the same concentration of Dox) at early time

points (15 and 30 min) was very weak and diffused throughout the cytoplasm; nuclear localization of Dox could only be seen at longer time points (120 min, Fig. 2). Confocal microscopy tracking the Dox uptake in live cells confirmed that the Dox/NG accumulated in Transferrin positive early endosomes within 15 min (seen as co-localized yellow punctate structures in Fig. 3A, merged panel) and trafficked into lysosomes within 30 min (as seen by colocalization with Lysotracker dye in Fig. 3B, merged panel).

As seen in the low-resolution microscopy images shown in Fig. 3, after 30 min incubation most of the fluorescence from Dox was within the cytosol and not the nucleus. However, by 60 min, the Dox fluorescence was found in the nucleus, confirming diffusion of Dox from the lysosomes. Lysosomal trapping of drug-loaded NGs is expected to modulate the release of the drug as well as control the degradation of the carrier. We have previously shown that Dox release rate from NGs is higher at the acidic pH, which is likely due to protonation of carboxylic groups of PGA and abating the drug and micelle electrostatic coupling. Since intracellular endocytotic vesicles are acidic (pH≈4.0 to 6.0), the transport of the NGs in these compartments can potentially trigger a release of a bolus of drug from the carrier. Degradation of the PGA-based NGs in the presence of lysosomal proteases such as cathepsin B or cleavage of reductively labile disulfide bonds in the NGs ionic cores can further facilitate the Dox release.

While the intrinsic fluorescence of Dox served as a method to follow the uptake of drug-loaded NGs and Dox-release, we followed ErbB2 degradation using a Western blot technique as a means to assess the release of 17-AAG and its ability to inhibit intracellular HSP90. The data shown in Fig. 4 clearly demonstrate that the encapsulated 17-AAG is released into the cytosol and can inhibit HSP90 leading to ErbB2-degradation.

As seen in Fig. 4A, 17AAG/NG or (Dox+17AAG)/NG induced ErbB2 degradation at the same level as the treatment with free 17-AAG in a dose-dependent manner. Notably, the kinetics of ErbB2 degradation were also comparable for NG-formulations and free 17-AAG (Fig. 4B).

Previous studies from our laboratory has shown that NGs with cross-linked ionic cores can be selectively endocytosed into cancer cells, which lack epithelial cell tight junctions, in contrast to normal epithelial cells that form tight junctions [38]. The internalization route appeared to be predominantly via the caveolar pathway. While the current studies report the ability of untargeted NGs to be internalized into ErbB2-overexpressing breast cancer cells, we anticipate that integration of targeting anti-ErbB2 antibody on to the surface of NGs could further facilitate selective delivery of their payload specifically into ErbB2-overexpressing breast cancer cells. In conjunction with passive targeting, ErbB2-targeted drug delivery should further reduce side effects of the chemotherapeutics. In contrast to the untargeted NGs, the ErbB2-specific uptake of the targeted NGs will be dictated by the ErbB2 endocytic pathway. However, one anticipated caveat is that the rate of Trastuzumab-induced ErbB2 internalization is very slow [28, 39]. Immunogold labeled electron microscopy has revealed that gold-labeled Trastuzumab can be detected within microvili-like protrusions and clathrin-coated pits at the cell surface as well as within recycling endosomes [39, 40]. We have shown that HSP90-inhibition induces ErbB2-ubiquitinylation,

resulting in accelerated internalization, ubiquitin-dependent sorting into multivesicular bodies and subsequent lysosomal-degradation [28]. Accordingly, we hypothesize that the uptake of the chemotherapeutic payload being delivered via ErbB2-targeted NGs can be significantly enhanced by concomitant treatment with HSP90-inhibitors, which can accelerate the internalization of the ErbB2-bound targeted drug cargo and routing them to the lysosomes leading to efficient drug-release and induction of cytotoxicity. These studies are ongoing in our laboratories and will be reported elsewhere.

In Vitro Cytotoxicity of Dox, 17-AAG or drug combination against ErbB2-high and ErbB2-low breast cancer cell lines

Dox is among the most active cytotoxic agents for the treatment of breast cancer. Dox induces DNA damage, and many DNA-repair components are HSP90 client proteins [41]. To test a hypothesis that 17-AAG contentment leads to sensitization of cancer cells to cytotoxic effects of Dox, we determined the cytotoxicity of various drug formulations in a panel of breast cancer cell lines with differential ErbB2 expression using MTT cell cytotoxicity assay (Supplementary Fig. 1–3). Calculated IC_{50} values (the concentration that inhibited cell growth by 50%) are summarized in Table 2.

We first confirmed that the Dox and 17-AAG combination at a 6:1 molar ratio (corresponding to the drug content encapsulated into NGs) was indeed synergistic in its cytotoxicity against high-level ErbB2-expressing BT-474 and 21MT-1 cell lines after concomitant treatment for 48 h. An approximately 6- and 18-fold reduction in the IC_{50} for Dox was seen in BT-474 and 21MT-1 cells, respectively, after treatment with drug combination. Chou-Talalay analysis of the data clearly indicated a combination index below 1 (such as 0.055 for BT-474 and 0.043 for 21MT-1) confirming strong pharmacological synergy. Similarly, we found that (Dox+17-AAG)/NG combination was significantly more effective in killing ErbB2-overexpressing cells than single Dox/NG formulation and displayed very pronounced synergistic cytotoxicity. The corresponding CI values of (Dox +17-AAG)/NG combination at IC_{50} were 0.043 and 0.06 for BT-474 and 21MT-1cells, respectively. On the other hand, no appreciable differences between the combination treatment and Dox alone (either free or loaded in NGs) were detected in similar experiments conducted on the ErbB2-low MCF-7 cells (Table 2), suggesting that 17-AAG plus Dox combination can induce synergistic anti-proliferative effects selectively in ErbB2-overexpressing breast cancer cells.

Anti-tumor activity of (Dox+17-AAG)/NG in ErbB2-driven xenograft model

Motivated by the enhanced *in vitro* efficacy of (Dox+17-AAG)/NG formulation, we evaluated its antitumor efficacy *in vivo* in ErbB2-driven xenograft model. Intravenous administrations of each formulation were given 4 times at 4-day intervals at an equivalent dose of 6 mg-Dox/kg. Animals injected with (Dox+17-AAG)/NG or free drug combination received 6mg/kg Dox and 1 mg/kg 17-AAG equivalents per dose. The changes in the relative tumor volume, body weight and animal lifespan are shown in Fig. 5A, 5B and 5C, respectively.

Tumor growth inhibition ratio between treated versus control groups (T/C value) was calculated on day 14 after treatment initiation according to the formula: T/C = $(V_t-V_o)_{\text{treated tumor}}/(V_t-V_o)_{\text{control tumor}}$, where V_t and V_o represent the mean tumor volume on the evaluation day and at the start of the experiment, respectively. Consistent with the *in vitro* findings, combination treatment with (Dox+17-AAG)/NG formulation resulted in a more significant tumor volume reduction (T/C = 0.13), which translated into increased overall survival of the animals compared to the animal groups treated with a combination of free drugs (Dox+17-AAG) at equivalent drug concentrations ($P<0.05$, Fig. 5A & 5C). Although not as prominent as (Dox+17-AAG)/NG formulation, tumor burden was also decreased by treatments with Dox alone (T/C = 0.54) or combination of free drugs (Dox +17-AAG, T/C = 0.47) or Dox/NG (T/C = 0.39) compared to control (Fig. 5A). Notably, survival of the animals treated with Dox/NG was higher than in animals treated with the combination of free drugs or Dox alone, which could be attributed to the pronounced systemic toxicity of (Dox+17-AAG) and Dox treatments (Fig. 5C). Figure 5B shows that animals treated with either single or binary drug-loaded NGs only lost ~5% body weight during the 2-week study period compared to control group while the same dose of Dox or the free drug combination (Dox+17-AAG) produced a considerable body weight loss (>15%, $P < 0.05$). These results indicate that Dox-loaded NGs have a much-improved therapeutic index when compared with free Dox. Notably, treatment with 17-AAG/NG did not have any substantial effect on the tumor growth (T/C = 0.87) and only minor increase in survival was observed over controls. To further corroborate the superior antitumor efficacy of binary drug combination in NGs, the tumors were excised post-treatment (on 10^{th} day after last injection) and processed for staining of Ki-67 to examine the effect of treatment on cell proliferation.

The number of Ki-67 positive cells were significantly lower in tumors from mice that received (Dox+17-AAG)/NG compared to tumors in control *(*$P<0.001$*)* or Dox+17-AAG *(*$P<0.01$*)* or Dox/NG *(*$P<0.05$*)* (Fig. 6A), which reflected the decrease in the size of the excised tumors (Fig. 6B). Light microscopic examination of H&E-stained tissue (liver, spleen, heart kidney and lung) sections from sacrificed animals (day 22) did not show any evidence of toxicity (data not shown). Collectively, these data provide *in vivo* evidence that biodegradable PEG-polypeptide NGs carrying Dox and 17-AAG drug combination exerted superior antitumor efficacy, both in terms of tumor inhibition and survival, which could be attributed to the preferential simultaneous accumulation, and increased potency.

4. Conclusions

Using an ErbB2-driven breast cancer model, we demonstrated the potential of PEG-polypeptide nanogels as novel nanocarriers for the delivery of synergistic combinations of chemotherapeutics with the HSP90 inhibitor, 17-AAG. Importantly, the binary drug combination of 17-AAG and Dox simultaneously delivered using NGs exhibited superior antitumor efficacy compared to a combination of free drugs and single drug NGs analogues. Inhibition of HSP90, which leads to degradation and down-regulation of several oncogenic client proteins, is a strategy being extensively explored as treatment for various types of cancers. HSP90 inhibitors, such as 17-AAG, which can synergize with various currently used anticancer agents has shown significant potential in initial phase II clinical trials,

including in ErbB2-driven breast cancers. We have previously demonstrated the potential of 17-AAG to synergize with Trastuzumab and induce cytotoxicity in ErbB2-driven breast cancer models. Our studies with biodegradable and biocompatible polymeric NGs provide an alternative to the formulation issues that have impeded the development of 17-AAG. Moreover, these nanocarriers provide an opportunity to encapsulate multiple drugs with various physicochemical properties and modes of action. While doxorubicin was chosen as a model chemotherapeutic in this study, we anticipate that the multidrug loaded NGs represent an attractive platform for the development of potent combinations of HSP90 inhibitors with cytotoxic agents and, thus, further investigations of these NGs are warranted.

Supplementary Material

Refer to Web version on PubMed Central for supplementary material.

Acknowledgements

This work was supported by DOD Breast Cancer Research Program (grant W81XWH-11-1-0166 grant to HB and TB), Nebraska DHHS LB506 and the National Institutes of Health (grants CA116552, CA99163, CA87986 and CA105489 to HB, CA96844 to VB; CA 116590 to TB). SMR acknowledges support from Nebraska Department of Health and Human Services and Center for Biomedical Research Excellence (CoBRE), Nebraska Center for Nanomedicine (COBRE-NCN; seed grant). We acknowledge the assistance of the Nanomaterials Core Facility of the COBRE-NCN supported by the Institutional Development Award (IDeA) from the National Institute of General Medical Sciences of the NIH grant number P20GM103480. We would like to thank the NMR and Confocal Microscopy Core Facilities at UNMC (supported by the NCI Cancer Center Support Grant to Buffett Cancer Center) for excellent technical assistance.

References

1. Slamon DJ, Godolphin W, Jones LA, Holt JA, Wong SG, Keith DE, Levin WJ, Stuart SG, Udove J, Ullrich A. Studies of the HER-2/neu proto-oncogene in human breast and ovarian cancer. Science. 1989; 244:707–712. [PubMed: 2470152]
2. Perou CM, Sørlie T, Eisen MB, van de Rijn M, Jeffrey SS, Rees CA, Pollack JR, Ross DT, Johnsen H, Akslen LA. Molecular portraits of human breast tumours. Nature. 2000; 406:747–752. [PubMed: 10963602]
3. Sørlie T, Tibshirani R, Parker J, Hastie T, Marron J, Nobel A, Deng S, Johnsen H, Pesich R, Geisler S. Repeated observation of breast tumor subtypes in independent gene expression data sets. Proc Natl Acad Sci U S. 2003; 100:8418–8423.
4. Sotiriou C, Neo S-Y, McShane LM, Korn EL, Long PM, Jazaeri A, Martiat P, Fox SB, Harris AL, Liu ET. Breast cancer classification and prognosis based on gene expression profiles from a population-based study. Proc Natl Acad Sci U S. 2003; 100:10393–10398.
5. Slamon DJ, Leyland-Jones B, Shak S, Fuchs H, Paton V, Bajamonde A, Fleming T, Eiermann W, Wolter J, Pegram M. Use of chemotherapy plus a monoclonal antibody against HER2 for metastatic breast cancer that overexpresses HER2. N Engl J Med. 2001; 344:783–792. [PubMed: 11248153]
6. Graus-Porta D, Beerli RR, Daly JM, Hynes NE. ErbB-2, the preferred heterodimerization partner of all ErbB receptors, is a mediator of lateral signaling. EMBO J. 1997; 16:1647–1655. [PubMed: 9130710]
7. Moasser MM. The oncogene HER2: its signaling and transforming functions and its role in human cancer pathogenesis. Oncogene. 2007; 26:6469–6487. [PubMed: 17471238]
8. Bailey TA, Luan H, Clubb RJ, Naramura M, Band V, Raja SM, Band H. Mechanisms of Trastuzumab resistance in ErbB2-driven breast cancer and newer opportunities to overcome therapy resistance. J Carcinog. 2011; 10:28. [PubMed: 22190870]
9. Hudis CA. Trastuzumab—mechanism of action and use in clinical practice. N Engl J Med. 2007; 357:39–51. [PubMed: 17611206]

10. Mimnaugh EG, Chavany C, Neckers L. Polyubiquitination and proteasomal degradation of the p185c-erbB-2 receptor protein-tyrosine kinase induced by geldanamycin. J Biol Chem. 1996; 271:22796–22801. [PubMed: 8798456]
11. Schulte TW, Neckers LM. The benzoquinone ansamycin 17-allylamino-17-demethoxygeldanamycin binds to HSP90 and shares important biologic activities with geldanamycin. Cancer Chemother Pharmacol. 1998; 42:273–279. [PubMed: 9744771]
12. Neckers L. Heat shock protein 90 is a rational molecular target in breast cancer. Breast Dis. 2002; 15:53–60. [PubMed: 15687645]
13. Modi S, Stopeck A, Linden H, Solit D, Chandarlapaty S, Rosen N, D'Andrea G, Dickler M, Moynahan ME, Sugarman S. HSP90 inhibition is effective in breast cancer: a phase II trial of tanespimycin (17-AAG) plus trastuzumab in patients with HER2-positive metastatic breast cancer progressing on trastuzumab. Clin Cancer Res. 2011; 17:5132–5139. [PubMed: 21558407]
14. Xu W, Mimnaugh E, Rosser MF, Nicchitta C, Marcu M, Yarden Y, Neckers L. Sensitivity of mature Erbb2 to geldanamycin is conferred by its kinase domain and is mediated by the chaperone protein Hsp90. J Biol Chem. 2001; 276:3702–3708. [PubMed: 11071886]
15. Basso AD, Solit DB, Munster PN, Rosen N. Ansamycin antibiotics inhibit Akt activation and cyclin D expression in breast cancer cells that overexpress HER2. Oncogene. 2002; 21:1159. [PubMed: 11850835]
16. Powers MV, Workman P. Targeting of multiple signalling pathways by heat shock protein 90 molecular chaperone inhibitors. Endocrine-Related Cancer. 2006; 13:S125–S135. [PubMed: 17259553]
17. Trepel J, Mollapour M, Giaccone G, Neckers L. Targeting the dynamic HSP90 complex in cancer. Nat Rev Cancer. 2010; 10:537–549. [PubMed: 20651736]
18. Münster PN, Basso A, Solit D, Norton L, Rosen N. Modulation of Hsp90 Function by Ansamycins Sensitizes Breast Cancer Cells to Chemotherapy-induced Apoptosis in an RB-and Schedule-dependent Manner See The Biology Behind: EA Sausville, Combining Cytotoxics and 17-Allylamino, 17-Demethoxygeldanamycin: Sequence and Tumor Biology Matters. Clin Cancer Res. 2001; 7:2228–2236. [PubMed: 11489796]
19. Georgakis G, Li Y, Younes A. Preclinical evaluation of the HSP-90 inhibitor 17AAG in Hodgkin's and non-Hodgkin's lymphomas: Induction of apoptosis and potentiation of chemotherapy cytotoxicity. Proc Annu Meet Am Soc Clin Onco. 2005:6570.
20. Sarangi U, Paithankar KR, Kumar JU, Subramaniam V, Sreedhar AS. 17AAG Treatment Accelerates Doxorubicin Induced cellular senescence: Hsp90 Interferes with enforced senescence of Tumor cells. Drug target insights. 2012; 6:19. [PubMed: 22915839]
21. Desale SS, Cohen SM, Zhao Y, Kabanov AV, Bronich TK. Biodegradable hybrid polymer micelles for combination drug therapy in ovarian cancer. J Control Release. 2013; 171:339–348. [PubMed: 23665258]
22. Godsey ME, Suryaprakash S, Leong KW. Materials innovation for co-delivery of diverse therapeutic cargos. RSC Adv. 2013; 3:24794–24811. [PubMed: 24818000]
23. Jong HSO, Kim Oh, Desale Swapnil, Kabanov Alexander V, Bronich Tatiana K. Polypeptide nanogels with hydrophobic moieties in the cross-linked ionic cores: synthesis, characterization and implications for anticancer drug delivery. J Drug Taget. 2013
24. Han Y, He Z, Schulz A, Bronich TK, Jordan R, Luxenhofer R, Kabanov AV. Synergistic combinations of multiple chemotherapeutic agents in high capacity poly (2-oxazoline) micelles. Mol Pharm. 2012; 9:2302–2313. [PubMed: 22681126]
25. Lee CC, Gillies ER, Fox ME, Guillaudeu SJ, Fréchet JM, Dy EE, Szoka FC. A single dose of doxorubicin-functionalized bow-tie dendrimer cures mice bearing C-26 colon carcinomas. Proc Natl Acad Sci U S A. 2006; 103:16649–16654. [PubMed: 17075050]
26. Band V, Zajchowski D, Swisshelm K, Trask D, Kulesa V, Cohen C, Connolly J, Sager R. Tumor progression in four mammary epithelial cell lines derived from the same patient. Cancer Res. 1990; 50:7351–7357. [PubMed: 1977518]
27. Raja SM, Clubb RJ, Ortega-Cava C, Williams SH, Bailey TA, Duan L, Zhao X, Reddi AL, Nyong AM, Natarajan A. Anticancer activity of Celastrol in combination with ErbB2-targeted

therapeutics for treatment of ErbB2-overexpressing breast cancers. Cancer Biol Ther. 2011; 11:263–276. [PubMed: 21088503]

28. Raja SM, Clubb RJ, Bhattacharyya M, Dimri M, Cheng H, Pan W, Ortega-Cava C, Lakku-Reddi A, Naramura M, Band V. A combination of trastuzumab and 17-AAG induces enhanced ubiquitinylation and lysosomal pathway-dependent ErbB2 degradation and cytotoxicity in ErbB2-overexpressing breast cancer cells. Cancer Biol Ther. 2008; 7:1630–1640. [PubMed: 18769124]
29. Ferrari M, Fornasiero MC, Isetta AM. MTT colorimetric assay for testing macrophage cytotoxic activity in vitro. J Immunol Methods. 1990; 131:165–172. [PubMed: 2391427]
30. Nukolova NV, Oberoi HS, Cohen SM, Kabanov AV, Bronich TK. Folate-decorated nanogels for targeted therapy of ovarian cancer. Biomaterials. 2011; 32:5417–5426. [PubMed: 21536326]
31. Scaltriti M, Dawood S, Cortes J. Molecular pathways: targeting hsp90—who benefits and who does not. Clin Cancer Res. 2012; 18:4508–4513. [PubMed: 22718860]
32. Mitsiades CS, Mitsiades NS, McMullan CJ, Poulaki V, Kung AL, Davies FE, Morgan G, Akiyama M, Shringarpure R, Munshi NC. Antimyeloma activity of heat shock protein-90 inhibition. Blood. 2006; 107:1092–1100. [PubMed: 16234364]
33. Ayrault O, Godeny MD, Dillon C, Zindy F, Fitzgerald P, Roussel MF, Beere HM. Inhibition of Hsp90 via 17-DMAG induces apoptosis in a p53-dependent manner to prevent medulloblastoma. Proc Natl Acad Sci U S A. 2009; 106:17037–17042. [PubMed: 19805107]
34. Georgakis GV, Li Y, Rassidakis GZ, Medeiros LJ, Younes A. The HSP90 inhibitor 17-AAG synergizes with doxorubicin and U0126 in anaplastic large cell lymphoma irrespective of ALK expression. Exp Hematol. 2006; 34:1670–1679. [PubMed: 17157164]
35. Lai C, Park K, Lee D, Alberobello A, Raffeld M, Pierobon M, Pin E, Petricoin E III, Wang Y, Giaccone G. HSP-90 inhibitor ganetespib is synergistic with doxorubicin in small cell lung cancer. Oncogene. 2013; 33:4867–4876. [PubMed: 24166505]
36. Arlander SJ, Eapen AK, Vroman BT, McDonald RJ, Toft DO, Karnitz LM. Hsp90 inhibition depletes Chk1 and sensitizes tumor cells to replication stress. J Biol Chem. 2003; 278:52572–52577. [PubMed: 14570880]
37. Spector NL, Blackwell KL. Understanding the mechanisms behind trastuzumab therapy for human epidermal growth factor receptor 2-positive breast cancer. J Clin Oncol. 2009; 27:5838–5847. [PubMed: 19884552]
38. Sahay G, Alakhova DY, Kabanov AV. Endocytosis of nanomedicines. J Control Release. 2010; 145:182–195. [PubMed: 20226220]
39. Austin CD, De Mazière AM, Pisacane PI, van Dijk SM, Eigenbrot C, Sliwkowski MX, Klumperman J, Scheller RH. Endocytosis and sorting of ErbB2 and the site of action of cancer therapeutics trastuzumab and geldanamycin. Mol Biol Cell. 2004; 15:5268–5282. [PubMed: 15385631]
40. Maier LA, Xu FJ, Hester S, Boyer CM, McKenzie S, Bruskin AM, Argon Y, Bast RC. Requirements for the internalization of a murine monoclonal antibody directed against the HER-2/neu gene product c-erbB-2. Cancer Res. 1991; 51:5361–5369. [PubMed: 1680547]
41. Kaplan KB, Li R. A prescription for ‘stress’–the role of Hsp90 in genome stability and cellular adaptation. Trends Cell Biol. 2012; 22:576–583. [PubMed: 22959309]

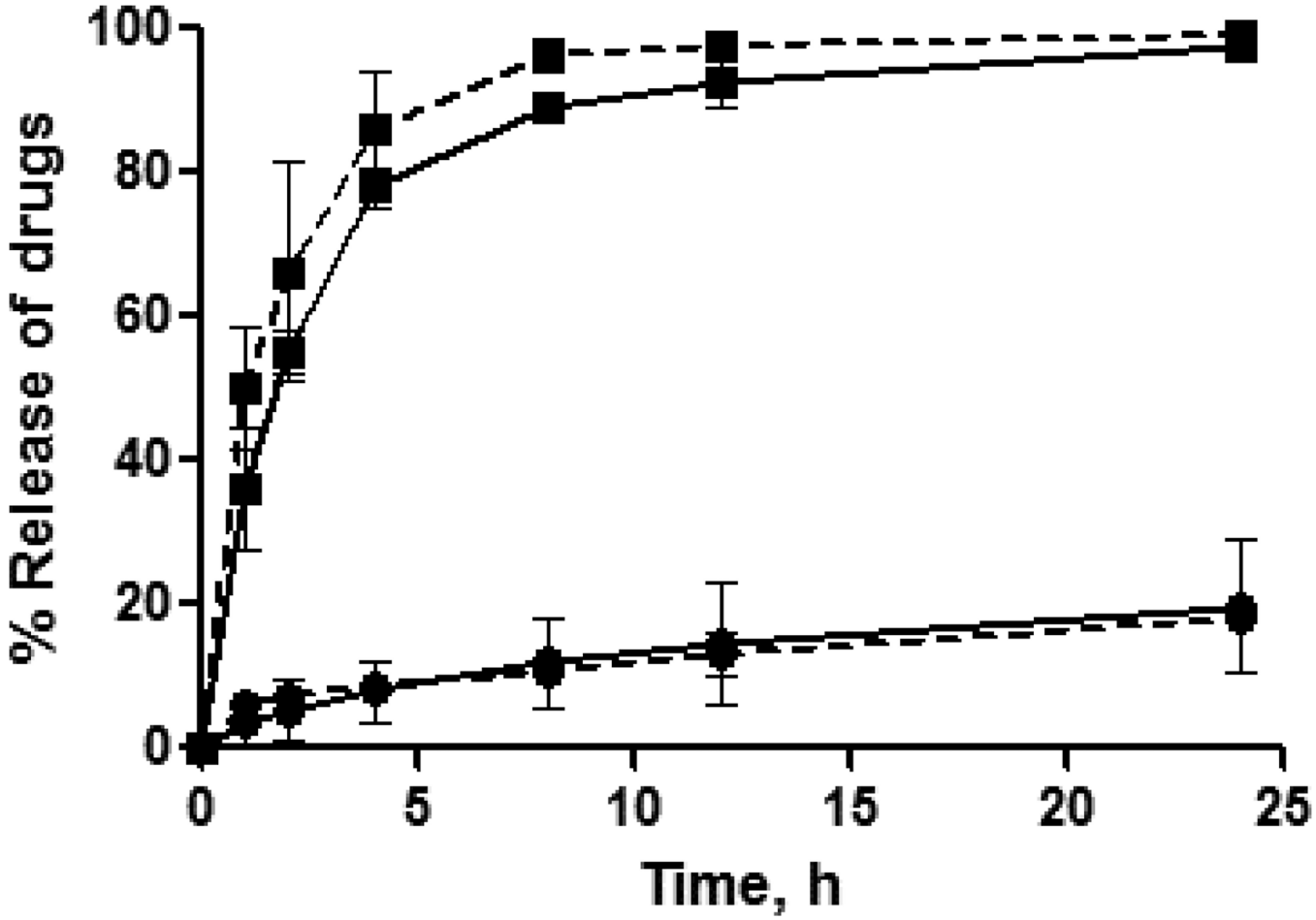

Fig. 1. Drug release profiles from single drug-loaded NGs (solid line) and binary drug combination-loaded NGs (dotted line) for Dox (●) and 17-AAG (■) in PBS buffer, pH 7.4

The loading amount of Dox for each sample is 200 μg. The data represent averaged values and standard deviations calculated based on three independent experiments.

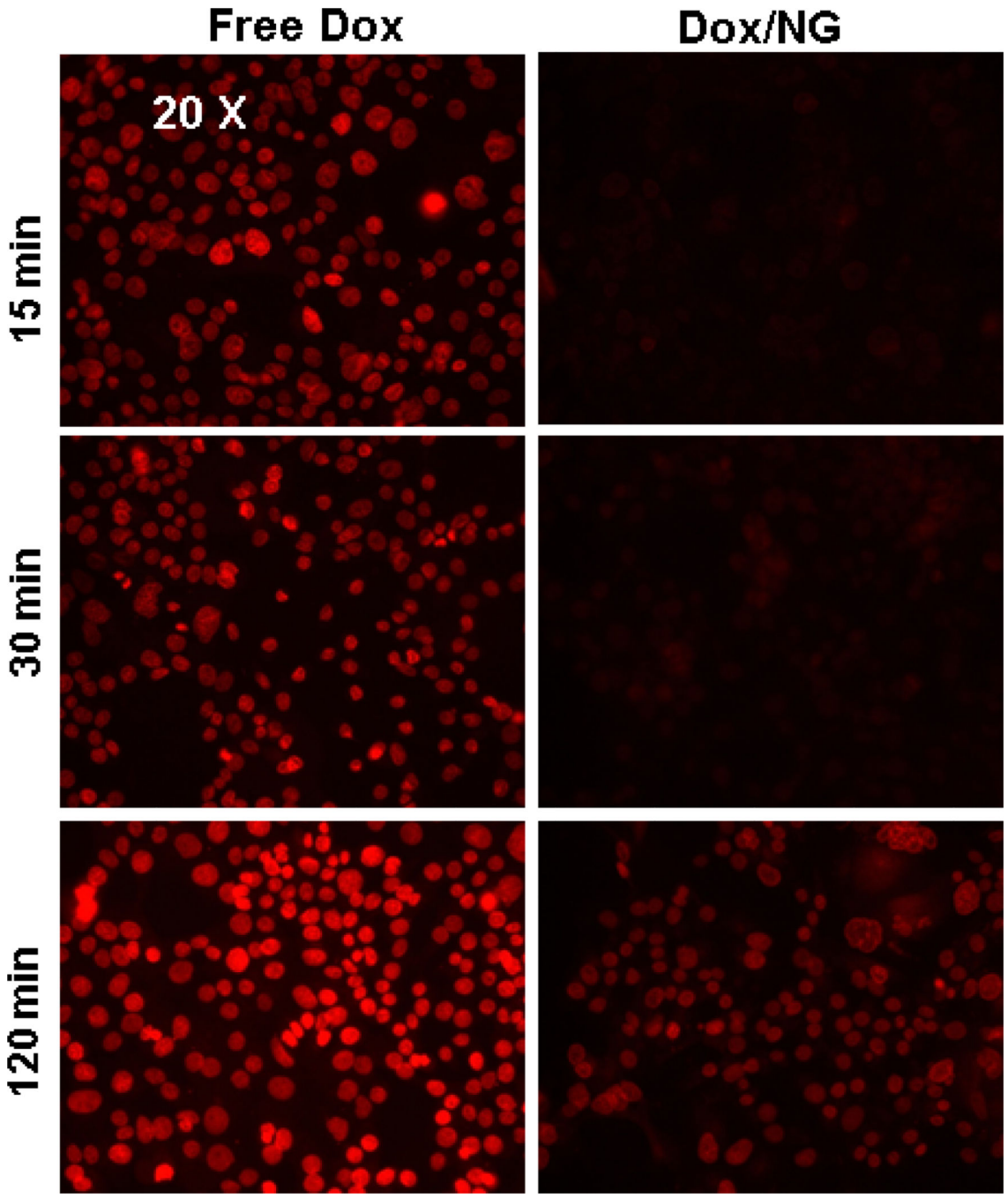

Fig. 2. Comparison of kinetics of cellular Dox distribution in ErbB2 overexpressing 21MT-1 cells after treatment with Free Dox or Dox/NG

Cells, grown on glass coverslips, were exposed to free Dox or Dox/NG (10 μg/mL Dox equivalents) for the indicated time periods following which the cells were washed 3X in PBS and fixed using 4% PFA for 20 min. The cells on the coverslips were then imaged using a regular fluorescence microscope, using a 20× objective. Shown here is a comparison of the distribution of Dox-fluorescence (red) within the cells, as a function of time, when added in the free form vs the NG-formulation.

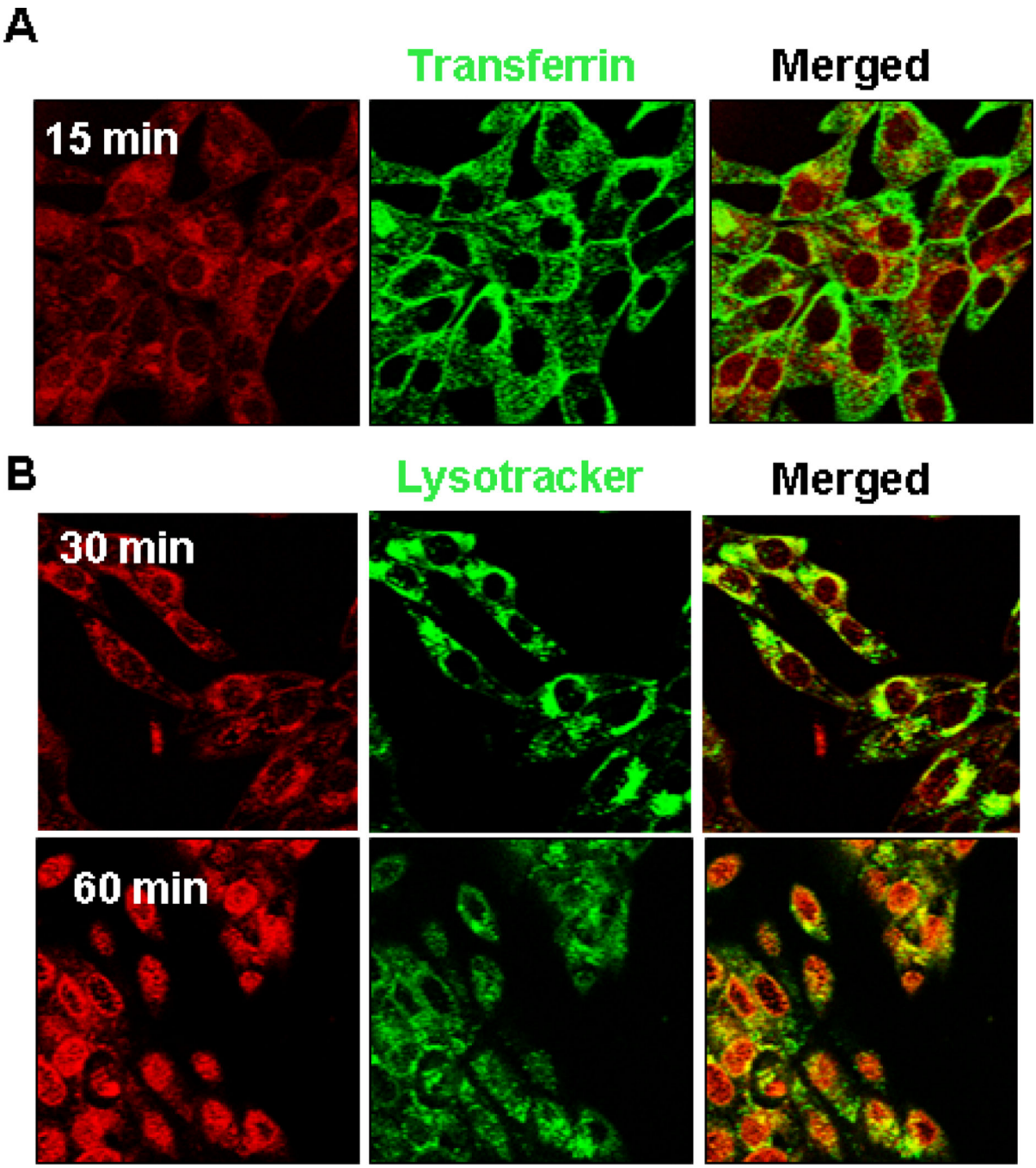

Fig. 3. Confocal immunofluorescence analysis of cellular distribution of Dox/NG

21MT-1 cells grown on coverslips were loaded with 10 μg/ml Alexa488-labeled transferrin (early endosomal marker) or Lysotracker Green (lysosomal marker; 100nM) for 10 min at 37°C. Dox/NG (10 μg/mL Dox equivalents) was then added and the uptake and intracellular distribution of Dox/NG (red) within Transferrin- or Lysotacker green-positive compartments, was followed using live cell imaging. Shown here the distribution of Dox fluorescence (red) within transferrin-positive (panel A) early endosomes after 15 min, and in

lysosomal compartment (lysotracker green positive) after 30 min (panel B). Clear nuclear localization is seen after 60 min of incubation.

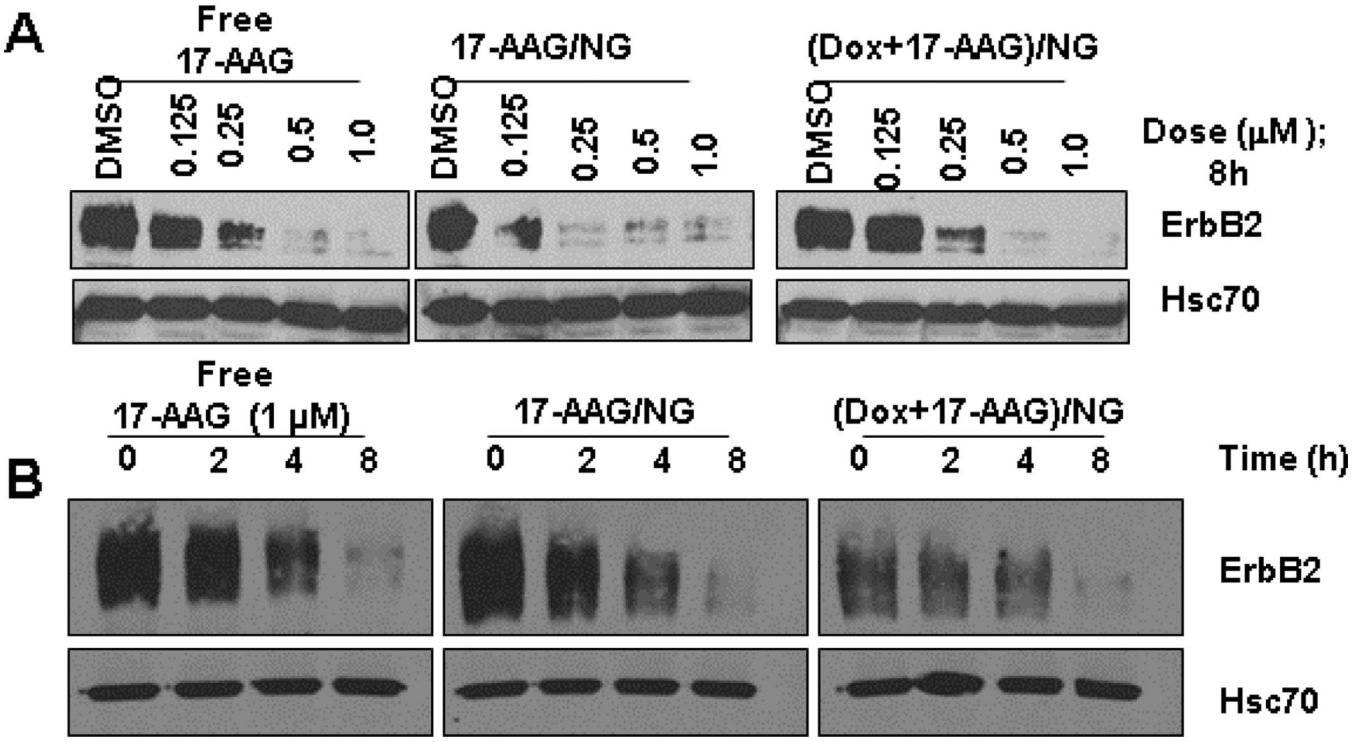

Fig. 4. 17-AAG-loaded NGs can induce ErbB2-degradation in 21MT-1 cell lines as efficiently as free 17 AAG

Cells were treated with the indicated concentrations of free 17-AAG or the NG-formulations for 8h (Dose response experiment; panel **A**) or with fixed concentration (1 μM) of free 17-AAG or the NG-formulations for the indicated time periods (kinetics; panel **B**). Samples were lysed in Triton X-100 lysis buffer and 25 μg aliquot of total protein was analyzed by SDS-PAGE/WB. Shown here are changes in ErbB2-levels as a result of HSP90-inhibition. Hsc70 is shown as loading control.

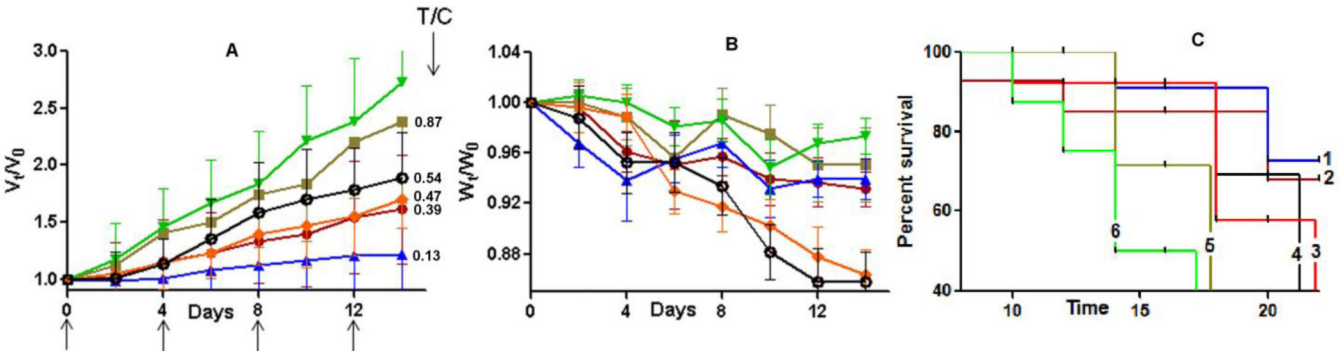

Fig. 5. In vivo antitumor efficacy of (Dox + 17-AAG)/NG in ErbB2+ - BT-474 breast cancer mice model

Relative changes in (A) tumor volume and (B) body weight were measured following intravenous administration of (Dox + 17-AAG)/NG (▲) or Dox/NG (●) or Dox + 17-AAG (♦) or Free Dox (Ø) or 17-AAG/NG (■) or 5% dextrose (▼). Drug formulations were injected in 100 μL at a dose of 6 mg Dox or 1mg 17-AAG equivalents/kg body weight 4 times at 4-day intervals as indicated by the arrows. Values indicated are means ± SEM (n = 10). (C) Kaplan–Meier analysis of overall survival in (Dox + 17-AAG)/NG group (1) or Dox/NG group (2) or Dox + 17-AAG group (3) or Dox alone (4) or 17-AAG/NG group (5) or control group (6). Tumor volume and body weight are normalized with respect to tumor volume or body weight at day 0. * $P<0.05$, ** $P<0.01$.

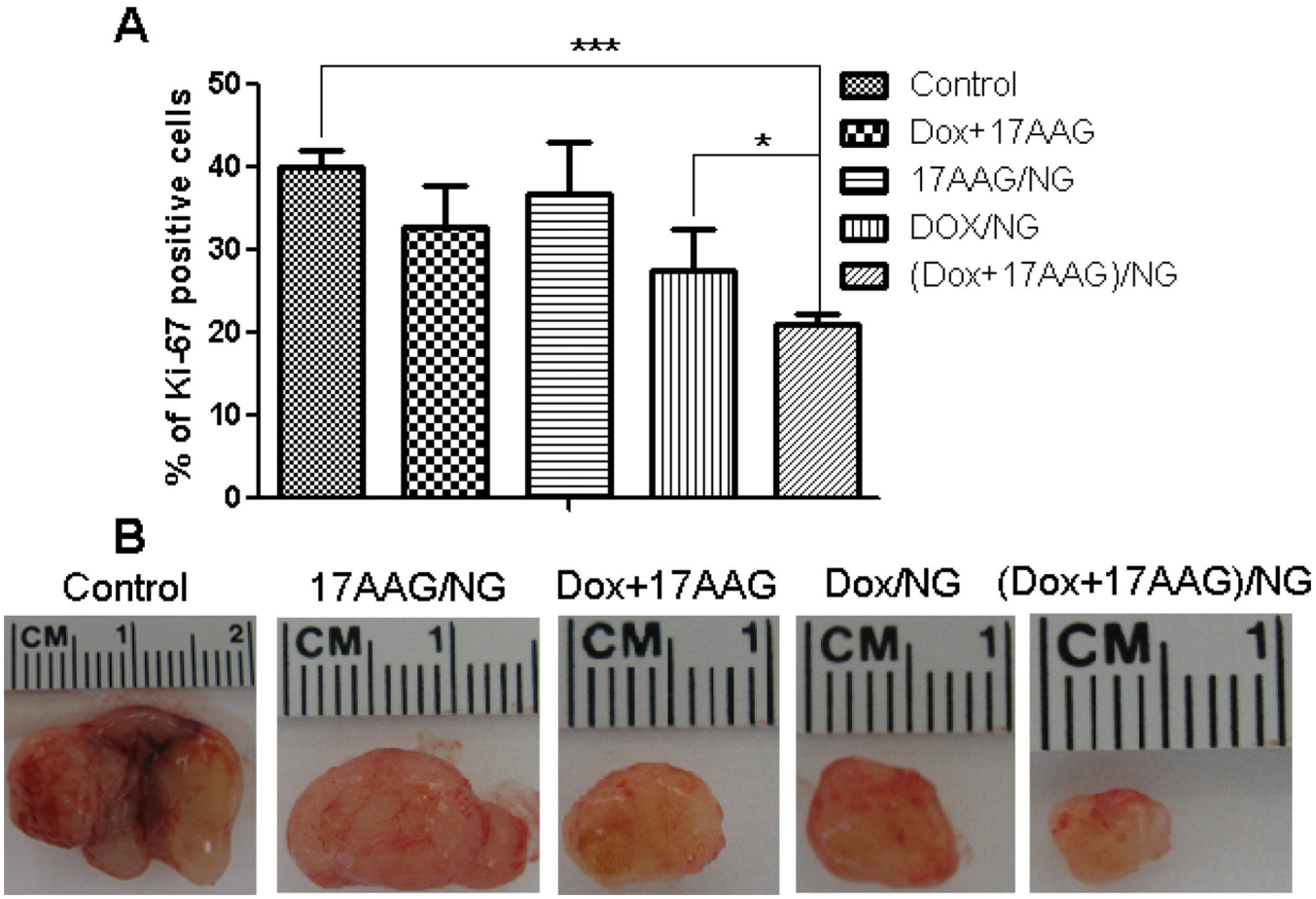

Fig. 6. Ki-67-caspase-3 apoptosis assay of excised tumors from mice treated with free drugs or NG-formulations

Panel **A** - Quantification of Ki-67 positive cells in tumor tissue from mice from various groups. Data are presented as mean ± SD (n = 5 random microscopic fields for each tumor slice). * $P<0.05$, *** $P<0.001$. Panel **B** shows a comparison of the tumor size for each treatment condition.

Table 1

Physicochemical characterization of NGs before and after drug loading[a]

Formulation	D_{eff} (nm)	PDI	ζ-potential (mV)	LC (% w/w)[b]	
				Dox	17-AAG
Empty NG	82 ± 1	0.18	−45.0 ± 5.2	-	-
Dox/NG	69 ± 2	0.20	−19.1 ± 1.5	18.1	-
17-AAG/NG	95 ± 1	0.17	−25.7 ± 1.7	-	2.7
(Dox+17-AAG)/NG	63 ± 5	0.16	−21.5 ± 0.47	18.1	3.1

[a] Effective diameter (D_{eff}), polydispersity index (PDI) and ζ-potential were determined in water (pH 6.5).

[b] Dox and 17-AAG content were determined by UV and HPLC, respectively. Loading capacity (LC) is expressed as mass of incorporated drug per mass of drug-loaded nanogels (w/w).

Table 2

Comparison of IC_{50} values for drug-loaded NGs and free drugs against various breast cancer cell lines as determined by the MTT assay.

Formulation	IC_{50} (μM) [with respect to Dox]		
	BT-474	**21-MT1**	**MCF-7**
Free Dox	0.60 ± 0.08	0.13 ± 0.17	0.65 ± 0.13
Free 17-AAG	0.011 ± 0.003	0.005 ± 0.002	0.09 ± 0.04
Free Dox + 17-AAG[a]	0.09 ± 0.03 (CI[b] = 0.055)	0.007 ± 0.002 (CI = 0.043)	0.63 ± 0.17 (CI = 0.85)
Dox/NG	2.40 ± 0.22	0.47 ± 0.20	1.05 ± 0.02
17-AAG/NG	0.022 ± 0.002	0.009 ± 0.003	0.14 ± 0.04
(Dox+17-AAG)/NG[a]	0.13 ± 0.05 (CI = 0.043)	0.08 ± 0.03* (CI = 0.060)	0.81 ± 0.18 (CI = 0.93)

[a] The molar ratio of DOX :17-AAG of 6:1 was used for the drug combination studies.

[b] CI values were calculated at IC_{50}.